

MODELLING THE PROPAGATION OF FORWARD AND OPPOSED SMOULDERING COMBUSTION

Guillermo Rein

School of Engineering and Electronics, University of Edinburgh, Scotland, EH9 3JL. UK
G.Rein@ed.ac.uk

Jose L. Torero

School of Engineering and Electronics, University of Edinburgh, Scotland, EH9 3JL. UK
J.Torero@ed.ac.uk

A. Carlos Fernandez-Pello

University of California at Berkeley, California 94720, USA
ferpello@me.berkeley.edu

Abstract. *A computational study has been carried out to investigate smouldering ignition and propagation in polyurethane foam. The one-dimensional, transient, governing equations for smouldering combustion in a porous fuel are solved accounting for improved solid-phase chemical kinetics. Forward and opposed smouldering modes are examined and the model describes well both propagation modes. Specifically, the model predicts the reaction-front thermal and species structure, the onset of smouldering ignition, and the propagation rate. This is a significant step forward in smouldering combustion modelling, because unification of forward and opposed propagation modes had never been achieved before. This breakthrough is associated to the use of improved chemical kinetics obtained with a novel methodology to establish the reaction chemistry. The corresponding kinetic parameters for a reduced five step mechanisms of polyurethane foam smouldering kinetics are used. These kinetic mechanisms are then used to model one-dimensional smouldering combustion, numerically solving for the solid-phase and gas-phase conservation equations. A forced flow of oxidizer gas is considered and gravity neglected. The results from previously conducted microgravity experiments with flexible polyurethane foam are used for calibration and testing of the model predictive capabilities.*

Keywords. *Fire, Kinetics, Multidimensional, Computational, Smolder*

1. Introduction

Smouldering phenomenon is a flameless form of combustion, deriving its heat from heterogeneous reactions occurring on the surface of a solid fuel when heated in an oxidizer environment (Ohlemiller 2002). It is of interest both as a fundamental combustion problem and as a practical fire hazard. Common examples of smouldering combustion are the initiation of residential fires in upholstered furniture by weak heat sources and the persistent burning of biomass behind the flaming front of a wildland fire.

Many materials can sustain a smouldering reaction, including coal, cotton, tobacco, paper, duff, peat, wood and charring polymers. In general, these fuels consist of an aggregate and permeable medium formed by particulates, grains, fibers or a porous matrix. The aggregate fuel elements facilitate the surface reaction with oxygen by providing a large surface area per unit volume. They also act as thermal insulation that reduces heat losses but, at the same time, permit oxygen transport to the reaction sites by convection and diffusion.

From a fundamental point of view, smouldering is a basic combustion problem involving heterogeneous chemical reactions, and the transport of heat, mass and momentum in the gas and solid phases. Smouldering initiation requires the supply of heat flux to the solid fuel. The subsequent temperature increase of the solid triggers its thermal-degradation reactions (endothermic pyrolysis and exothermic oxidation) until the net heat released is high enough to balance the heat required for propagation. This net heat released is transferred by conduction, convection and radiation partially ahead of the reaction and partially lost to the surrounding environment. The oxidizer is transported to the reaction zone by diffusion and convection, in turn feeding the oxidation reactions. Once ignition occurs, the smoulder reaction propagates through the material in a creeping fashion. It has been observed that for most materials and typical conditions, the two limiting factors in smouldering propagation are the oxidizer flux to and the heat losses from the reaction zone.

2. Multidimensional Propagation and Chemical Kinetics

When studying smoulder propagation through the interior of combustible materials, it is common to consider the simpler one-dimensional process and to classify it in two main configurations; opposed and forward propagation. These are defined according to the direction in which the smoulder reaction propagates relative to the oxidizer flow; in opposed smoulder, the reaction front propagates in the direction opposite to the oxidizer flow, and in forward smoulder, the front propagates in the same direction. A common case of forward smoulder is a burning cigarette being puffed.

These two modes are distinguished by the roles played by the transport mechanisms and chemical reactions. In forward propagation, the fresh oxidizer flows through the char, reacts at the smoulder zone and then the oxidizer-depleted flow goes through the virgin fuel. This configuration favors that the oxidation reactions that occur at the char side of the smoulder zone and pyrolysis at the foam side. Convective transport is in the direction of the virgin fuel ahead, preheating it before the smoulder zone arrives. In opposed propagation, the fresh oxidizer flows through the virgin fuel and reacts at the smoulder zone. Convective transport is in the direction of the char behind the front, reducing the preheating of the fuel. Oxidation and pyrolysis occur both at the foam side of the smoulder reaction. Heat transfer in opposed propagation is upstream by conduction and radiation and downstream by convection. These modes tend to balance each other and thus opposed propagation is steady, while in forward propagation all three modes of heat transfer preheat the foam, therefore is unsteady in nature and propagates at a faster rate. In two- and three-dimensional propagation, the classification of all the possible configurations becomes a tedious task. In multidimensional smouldering, the propagation mode can no longer be classified in forward or opposed but a combination of both; where in instances one particular mode could be the dominant.

One of the biggest impediments preventing an increased usage of smoulder models for predictions is the current limited ability to characterize practical materials in terms of their thermal and oxidative degradation. Even for the most-studied case of cellulose, the chemical mechanisms involved in smouldering are too complex and not yet fully understood. The propagation rate of self-sustained smouldering is typically controlled by oxygen transport and net heat losses. Yet, heterogeneous chemical kinetics governs the front structure and dictates the effective value of the global heat of combustion. Chemical kinetics is particularly important for the kinetically controlled regimes of ignition, extinction, and the transition to flaming. In addition to the thermophysical aspects of smouldering, kinetics are also ultimately responsible in determining under what conditions a material ignites and smoulders.

Proper understanding and modelling of the combustion require information on the heterogeneous reactions taking place in the solid. Conventional models of smouldering use different kinetic schemes depending on the propagation mode. This limitation arises because, as mention before, the dominant thermal and kinetic mechanisms are different for forward than for opposed propagation. Thus, when reducing the combustion chemistry to an insufficient number of steps, the proposed kinetic schemes differ for each mode. From previous studies (see Rein 2006b for a review), it is seen that one and two are an insufficient number of steps to unify smouldering combustion. In this paper, a novel computational study is carried out to investigate the unification of forward and opposed propagation using a 5-step kinetic mechanism.

3. Microgravity Experiments

Experiments in the absence of gravity allow the development of new insights into the fundamental phenomena of smouldering combustion and offer unique experimental capabilities to establish an ideal flow environment (Law and Faeth 1994). In microgravity conditions there are no buoyant flows complicating the identification of the controlling mechanism, nor triggering the onset of turbulence and additional unsteadiness. Furthermore, microgravity environments provide ideal benchmark cases against which existing theories and new theories can be tested. These theories often neglect buoyancy effects and/or assume one-dimensional flow in situations where in reality buoyant effects induce two- or three-dimensional behavior. Microgravity continues to offer the unique ability to test truly one-dimensional flow experiments in combustion science. Previous studies have shown that complex buoyant recirculation flows can be established inside the porous media during the propagation of a smouldering reaction (Torero *et al.* 1993, Torero and Fernandez-Pello 1996). These flows are a function of the permeability and strongly influenced by thermal conditions of the reaction front. This complex scenario coupling momentum and energy transfer is not conducive to a fundamental validation study, thus microgravity experiments are preferred for the comparison. A numerical model of smouldering in microgravity does not need to model the buoyant transport of heat and mass inside the porous fuel and thus is simpler and needs fewer assumptions. In this paper, the results from previously reported microgravity experiments (Bar-Ilan *et al.* 2004a and 2004b) with polyurethane (PU) as fuel sample are used for testing our the modelling results.

4. Numerical Model

To date, no study has attempted to simulate both forward and opposed smouldering with the same kinetic mechanism and same kinetic parameters. Since there are no fundamental kinetic differences between opposed and forward smouldering combustion, the same appropriate kinetic scheme should describe adequately both forms.

The computational domain is shown in Fig. 1, which reproduces the setup in the microgravity experiments. The ignition is attempted at the boundary. Air is forced at one boundary and then flows through the domain. For opposed propagation, air is forced at the boundary, while for forward propagation air is forced at the boundary.

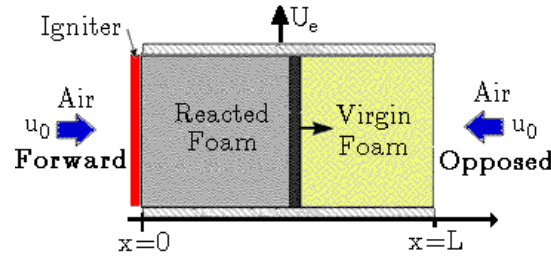


Figure 1: Computational domain for opposed and forward smouldering combustion.

A common difficulty in the application of models involving solid degradation is the lack of quantified kinetic behaviour. In order to overcome this difficulty, a systematic methodology for its determination, suitable for numerical models, is applied here to polyurethane foam. This methodology consists in the correlation of a mathematical representation of a reactive mechanism with data from thermogravimetric experiments using a genetic algorithm. This methodology has allowed the determination of the kinetic parameters of a new mechanism of polyurethane foam.

The model solves the one-dimensional transient equations for the solid and the gas. Only the essentials of the model are presented here and details and further results can be found in (Rein 2005). It consists of the conservation of energy of the solid (Eq. 1), solid species (Eq. 2 for each species j), energy of the gas (Eq. 3), continuity of the gas (Eq. 4) and gas species (oxygen is Eqs. 5 and smouldering products is Eq. 6).

$$\frac{\partial h_s'''}{\partial t} = \frac{\partial}{\partial x} \left(k_s \frac{\partial T}{\partial x} \right) + h_{gs} \frac{A_{gs}}{V} (T_g - T_s) - U_e \frac{A_L}{V} (T_s - T_0) - \rho_0 \sum_i \dot{\omega}_i \Delta h_i \quad (1)$$

$$\frac{\partial m_j}{\partial t} = \sum_i \dot{\omega}_j v_{j,i} \quad (2)$$

$$\frac{\partial}{\partial t} (\phi h_g''') = \frac{\partial}{\partial x} \left(\phi k_g \frac{\partial T_g}{\partial x} \right) + \frac{\partial}{\partial x} \left(\phi \rho_g \frac{K}{\mu} \frac{\partial p}{\partial x} c_{pg} (T_g - T_0) \right) - h_{gs} \frac{A_{gs}}{V} (T_g - T_s) \quad (3)$$

$$\frac{\partial}{\partial t} (\phi \rho_g) = \frac{\partial}{\partial x} \left(\phi \rho_g \frac{K}{\mu} \frac{\partial p}{\partial x} \right) + \rho_0 \sum_i \dot{\omega}_i v_{g,i} \quad (4)$$

$$\frac{\partial}{\partial t} (\phi \rho_g y_{O_2}) = \frac{\partial}{\partial x} \left(\phi \rho_g \frac{K_x}{\mu} \frac{\partial p}{\partial x} y_{O_2} \right) + \frac{\partial}{\partial x} \left(\phi \rho_g D_{diff} \frac{\partial y_{O_2}}{\partial x} \right) - \rho_0 \sum_i \dot{\omega}_i v_{O_2,i} \quad (5)$$

$$\frac{\partial}{\partial t} (\phi \rho_g y_{gp}) = \frac{\partial}{\partial x} \left(\phi \rho_g \frac{K_x}{\mu} \frac{\partial p}{\partial x} y_{gp} \right) + \frac{\partial}{\partial x} \left(\phi \rho_g D_{diff} \frac{\partial y_{gp}}{\partial x} \right) + \rho_0 \sum_i \dot{\omega}_i v_{gp,i} \quad (6)$$

Darcy's law has been used for the conservation of momentum, computing the gas velocity as a linear function of the pressure gradient in the porous medium. Buoyancy-induced flows are not modeled and thus the simulations are in microgravity conditions. The temperatures of the solid and the gas phases are calculated from the corresponding enthalpies using the specific heats. The pressure of the gas is calculated using the ideal gas law.

The 5-step mechanism for PU proposed by Rein *et al.* 2006 is used here. The mechanism consists of: two foam-pyrolysis reactions (Eqs. 7 and 8); two foam oxidation reactions (Eqs. 9 and 10); and one char oxidation reaction (Eq. 11), accounting for four solid species: foam, β -foam, char and residue, and two gas species; oxygen and products of smouldering.



The reaction rates for each one of the paths described above are expressed in the Arrhenius form and the kinetic parameters are obtained elsewhere (Rein *et al.* 2006). It is important to note that five steps were necessary to describe the kinetic behavior observed in the thermo-gravimetric experiments for PU and is a critical extension to earlier models that incorporated one reaction for opposed, and two or three for forward smoulder.

The conductivity of the solid includes the radiative conductivity in the optically thick limit. The effect of the heat losses in the perpendicular direction is accounted for in an approximate way as a volumetric heat-loss coefficient

(analytically calculated to be $0.3 \text{ W/m}^2\text{K}$ (Bar-Ilan *et al.* 2004b). The heat transfer between the gas phase and the solid phase is quantified to be in the order of $100 \text{ W/m}^3\text{K}$ (Rein 2005), which is high enough to imply virtual thermal equilibrium between the gas and the solid during smouldering (as the results show). The properties of the solid phase are weight averaged for the four solid species. The properties of the gas phase are approximated to those of air except for the molecular weight that is calculated based on typical PU smouldering products. The values for the most important parameters in the model are shown in Table 2.

At $t = 0$, the entire fuel bed is unreacted and the solid and gas are at ambient temperature. The boundary conditions as set imitating the conditions in the experiments. The heat-flux imposed by the igniter is such that the temperature rise with time at the igniter location is the same as in the experiments (ignition time of 600 s with a final igniter temperature of $480 \text{ }^\circ\text{C}$ for the opposed case, and ignition time of 400 s with a final temperature of $400 \text{ }^\circ\text{C}$ for the forward case). The thermal boundary condition after the ignition protocol is that heat is lost to the exterior resulting in the same cooling effect as seen in the experiments. As in the experiments, during the ignition, the inlet flow velocity is 0.01 mm/s . After ignition, the inlet forced-flow velocity is set to the corresponding nominal value and kept constant at the boundary thereafter.

The spatial partial derivatives in the governing equations are discretized using explicit finite-differences in a uniform grid whose nodes are in length. The state variables are defined at the center of each node and the velocities at the edges of each node. The grid-independence study is arguably the most reliable way to check if a numerical solution is accurate. Different solutions were computed for different-sized grids in order to find the relationship between the grid and the results. The error in the temperature profile computer with a given grid is defined as the integral of the square of the difference respect to the solution with a grid of 2000 nodes (in opposed propagation with 3 mm/s airflow). The convergence of the results as the grid is increased is demonstrated (see Fig. 2). The study concludes that a grid of 500 nodes provides satisfactory accuracy.

Suitable thermochemistry values for the smouldering combustion of PU are not available in the literature, and thus the parameters are determined through calibration and comparison of the numerical results with the experiments. The values found for the thermochemistry parameters are reported in (Rein *et al.* 2006).

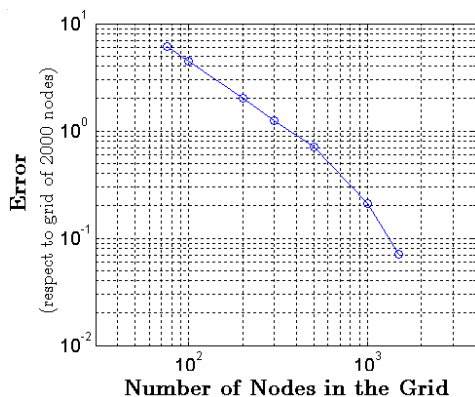


Figure 2: Results of the grid-independence study showing the convergence of the solution as the grid size increases

Table 1: Values of the most important parameters in the model.

Parameter	Value	Units
D	0.12	m
L	0.14	m
ρ_0	30	kg/m^3
ϕ_0	0.97	-
c_s	1760	J/kg
K_f	$5.2 \cdot 10^{-9}$	m^2
K_c	$3 \cdot 10^{-8}$	m^2
k_s	$3.4 \cdot 10^{-2}$	W/mK

5. Results

Both forward and opposed smouldering configurations are examined with the numerical model and new kinetics. Results for the computed solid temperature profiles are shown in Figs. 3 and 4. For the opposed case, the smouldering peak-temperature is $380 \text{ }^\circ\text{C}$ with a propagation velocity of 0.12 mm/s . The smouldering peak-temperature for the forward case is $430 \text{ }^\circ\text{C}$, and the propagation velocity is 0.21 mm/s . In forward propagation, the temperature profiles shows a dip moving ahead of the front that is caused by the endothermic pyrolysis. This dip is not present in the opposed propagation. A direct comparison with the previous microgravity experiments conducted aboard the Space Shuttle show that the model predicts successfully the experimental data in both opposed and forward propagation configurations. It is worth noting that the comparison excellent both in space and time, and remarkable for a one-dimensional model.

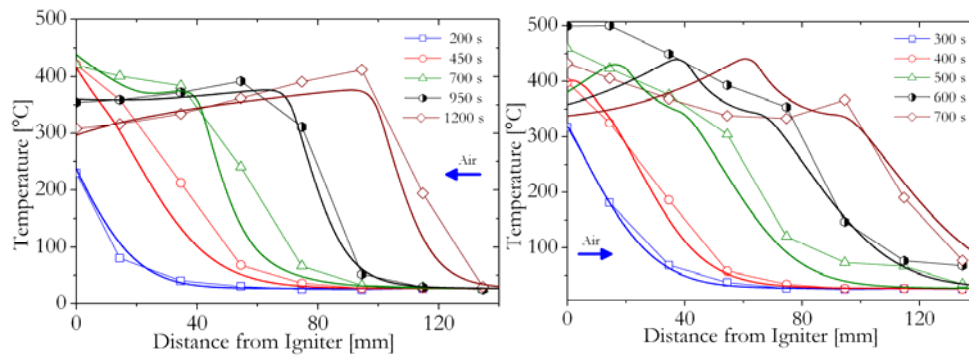


Figure 3. Temperature profiles of the solid vs. distance from igniter at different times; left) opposed smouldering with an inlet airflow of 3 mm/s; and right) forward smouldering with an inlet airflow of 5 mm/s. Comparison of numerical results (line) with experimental results (symbol with line).

As predicted by the model, modifications in the ignition protocol can have a significantly effect in the thermal penetration of the front. In order to compare to the transient measurements from the experiments, it is important to match the thermal and flow boundary conditions of the model.

The forward case is the most difficult to model because of the convective downstream influence of the igniter boundary condition and also because the on-set of secondary char-oxidation in the experiment. This reaction is observed in the experiment at 600 s taking place within the 40 mm next to the igniter producing higher temperatures and convecting heat downstream. Because it is not included in the 5-step mechanism, the model predicts lower temperatures after 600 s.

The temperature fields of the propagating fronts can be also seen in Fig. 4. These plots show the isotherms as a function of time and space. The slope of each contour line gives the propagation velocity. In the opposed case, the velocity is moderately constant in time and uniform in space after ignition. This indicates that the thickness of the smouldering front is constant during the process. In the forward case, the velocity is moderately constant in time but it can be observed that the contour lines diverge in space after ignition. This indicates that in forward propagation the thickness of the reactive front grows as the reaction progresses.

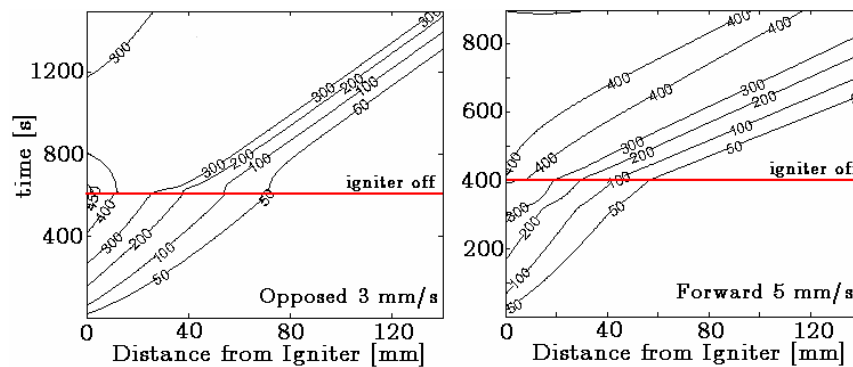


Figure 4. Numerical results for temperature contour lines as a function of time and space. Left) Opposed smouldering with an inlet airflow of 3 mm/s; and right) forward smouldering with an inlet airflow of 5 mm/s. The slope of each contour lines gives the propagation velocity.

As an example, the time profiles of four variables in opposed smouldering are presented in Fig. 5. The solid temperature profiles (Fig. 5a) show that the smouldering reaction is initiated at $t = 700$ s and that it propagates against the airflow from the igniter to the other end of the sample in 900 s. The oxygen mass fraction profiles (Fig. 5b) show that during ignition, the transport of oxygen to the igniter is dominated by diffusion (straighter curves), whereas after ignition the higher airflow imposed at the boundary makes convective transport to dominate (s-shape curves). The oxygen profiles also show that the smouldering reaction is oxygen starved during the later stages of the ignition and during the whole propagation. The pressure profiles (Fig. 5c) show that the pressure gradient is nearly constant along the sample except for a bump at the smoulder front. This drop is caused by the gases released from the reacting solid, which increase the gas velocity to roughly two times its value at the boundary. The solid mass profiles (Fig. 5d) show that about 70% of the solid reacts and that during ignition the solid consumption is higher. For all cases simulated, the maximum temperature difference between the solid and the gas was lower than 3°C , which implies that both phases are in virtual thermal equilibrium.

Results of the spatial profiles for the reaction rates, temperature and oxygen concentration at the smouldering front are presented in Fig. 6 (left of opposed, right for forward). It is seen that the model predicts that both fronts consume all the incoming oxygen. Considerable differences can be observed in the smoulder-front structure for the two propagation

modes. In opposed smouldering combustion, the oxidation and the pyrolysis reactions overlap to form one single front. This is consistent with experimental observations, where the propagation front appears as one single smoulder-front (Bar-Ilan *et al.* 2004b, Torero *et al.* 1993). The pyrolysis front combines contributions from the endothermic degradation of the foam and the β -foam. The oxidation front also has contributions from both, but it is dominated by the exothermic degradation of the β -foam. The starvation of oxygen occurs before the char oxidation is complete and results in little heat released by this reaction (also in agreement with experimental observations (Bar-Ilan *et al.* 2004b, Torero *et al.* 1993). The model predicts that both the pyrolysis and the oxidation fronts propagate at the same velocity in opposed smouldering (as Fig. 4 also indicates).

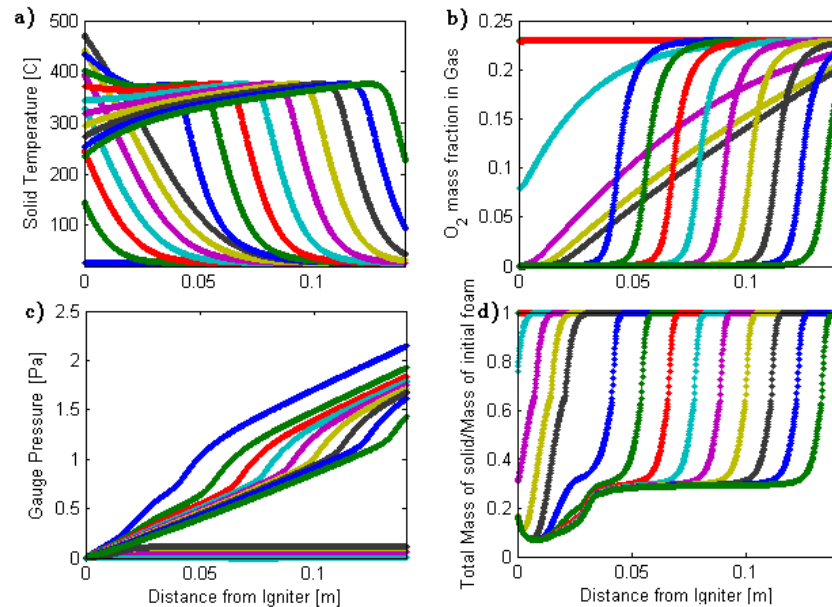


Figure 5: Numerical results vs. distance from igniter for opposed smouldering with 3 mm/s airflow. Each line is a different time in increments of 100s. a) Temperature of the Solid; b) Oxygen mass fraction in the gas; c) Pressure; d) Solid mass.

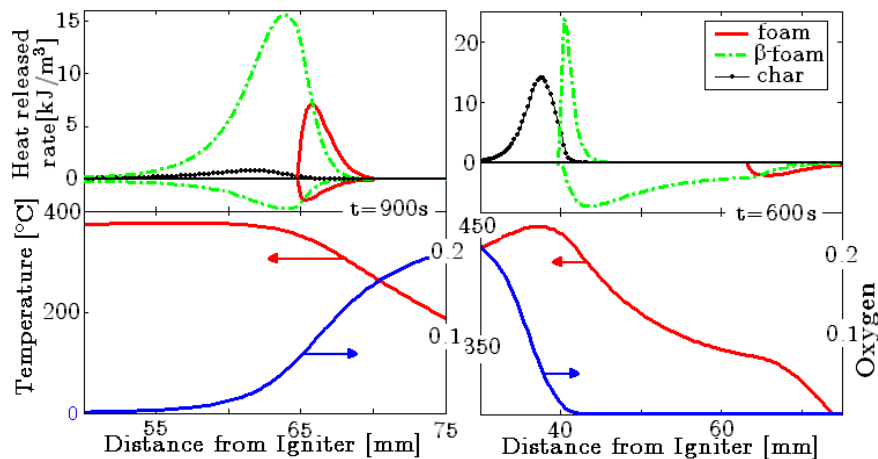


Figure 6. Numerical results for the front structure during self-propagation for; left) opposed smouldering; and right) forward smouldering. Top figures show the heat-released rate of each reaction (positive for oxidation, negative for pyrolysis). Bottom figures show the temperature and oxygen profiles.

The structure in forward smouldering combustion is quite different. The reactions form two distinct propagating fronts, the pyrolysis front being followed by the oxidation front. This result is also in agreement with experimental observations of forward propagation (Bar-Ilan *et al.* 2004a, Torero and Fernandez-Pello 1996). The pyrolysis front combines both the endothermic degradation of the foam and the β -foam, but the former dominates. Forward smouldering combustion results in virtually no oxidation of the virgin foam, as all of it is converted to β -foam via pyrolysis, but has strong β -foam oxidation. The hot char region receives the fresh supply of oxidizer so the char oxidation is vigorous, and all the char is converted to solid residue. The model predicts that the pyrolysis front propagates about 0.07 mm/s faster than the oxidation front (as the slopes in Fig. 4 also indicate). This finding was reported by Torero and Fernandez-Pello (1996) as an observation in their experiments, and it is due to the thermal wave traveling at a faster velocity than the oxidation wave.

The effect of the inlet airflow on the self-sustained propagation velocities was studied. Forward smouldering propagation is about 30% faster than opposed for the same inlet air velocity in the airflow range from 0 to 12 mm/s. The model predicts a sudden extinction of opposed smouldering combustion due to over-blowing. This extinction mechanism is not observed in forward mode for the range of airflow from 0 to 12 mm/s.

5. Conclusions and Final Remarks

The model presented here accounts for the most complete and fundamental description of smouldering combustion to date. The results from previously conducted experiments in microgravity are used for testing the numerical results. The model describes well both opposed and forward ignition and propagation. Specifically, the model predicts the reaction-front thermal and species structure, the onset of smouldering ignition, the propagation rate and the temperature profiles. Despite the simplicity associated to a one-dimensional model, the predictions reproduce extremely well the transient experimental results.

Microgravity environments provide ideal benchmark cases against which existing theories and new theories can be tested. Thus, the results from this model allow drawing conclusions on the role of each reaction and each heat transfer mode in the propagation of smouldering. Moreover, the model is used to explain experimental observations.

The present chemical mechanism makes possible the prediction of the experimental observations for both opposed and forward propagation. This is a significant step forward in the development of numerical models for smouldering combustion because the unification of forward and opposed propagation modes had never been achieved before. This is particularly relevant for multidimensional simulations where the classification between forward and opposed propagation is no longer possible.

6. Acknowledgement

This work was supported by the National Aeronautics and Space Administration, under grant NAG3-2026. The authors thank Dr. David Urban for his constant support and help.

7. References

- Bar-Ilan, A., G. Rein, A.C. Fernandez-Pello, J.L. Torero, D.L. Urban, 2004a, "Forced Forward Smoldering Experiments in Microgravity", *Experimental Thermal Fluid Science* 28, pp. 743-751.
- Bar-Ilan, A., G. Rein, D.C. Walther, A.C. Fernandez-Pello, J.L. Torero, D.L. Urban, 2004b, "The effect of buoyancy on opposed smoldering", *Combustion Science and Technology* 176, pp. 2027-2055.
- Law, C.K., G.M. Faeth, 1994, Opportunities and challenges of combustion in microgravity, *Progress in Energy and Combustion Science* 20 (1), pp. 65-113.
- Ohlemiller, T.J., 2002, *Smoldering Combustion*, SFPE Handbook of Fire Protection Engineering (3rd Ed.), Chp 2, pp. 200-210.
- Rein, G., 2005, *Computational Model of Forward and Opposed Smoldering Combustion with Improved Chemical Kinetics*, PhD. Thesis, Univ. of California at Berkeley. <http://repositories.cdlib.org/cpl/fs/ReinPhD05>.
- Rein, G., C. Lautenberger, A.C. Fernandez-Pello, J.L. Torero, D.L. Urban, 2006a, "Application of Genetic Algorithms and Thermogravimetry to Determine the Kinetics of Polyurethane Foam in Smoldering Combustion", *Combustion and Flame* 146 (1-2), pp. 95-108.
- Rein, G., A.C. Fernandez-Pello, D.L. Urban, 2006b, "Computational Model of Forward and Opposed Smoldering Combustion in Microgravity", *Proceeding of the Combustion Institute* 31 (2), pp. 2677-2684.
- Torero, J.L., A.C. Fernandez-Pello, 1996, "Forward smolder of polyurethane foam in forced air flow", *Combustion and Flame* 106, pp. 89-109.
- Torero, J.L., A.C. Fernandez-Pello, M. Kitano, 1993, "Opposed forced flow smoldering of polyurethane foam", *Combustion Science and Technology* 91, pp. 95-117.

8. Nomenclature

A_{gs}/V	Ratio of surface area between gas and solid to volume
A_L/V	Ratio of lateral area to volume
c	Specific heat
Δh	Enthalpy of reaction
h'''	Enthalpy per unit volume
h_{gs}	Heat transfer coefficient between gas and solid
K	Permeability
k	Conductivity
L	Sample length

- P Pressure
- T Temperature
- u Velocity
- U_e Global heat-loss coefficient to exterior
- y Mass fraction of gas species

Greek letters

- ν Mass yield/consumption of species per mass of reactant
- ρ Density
- σ Stephan-Boltzmann constant
- ϕ Porosity of the media
- $\dot{\omega}$ Reaction rate